

Optimization of micro heat exchanger: CFD, analytical approach and multi-objective evolutionary algorithms

Kwasi Foli, Tatsuya Okabe, Markus Olhofer, Yaochu Jin, Bernhard Sendhoff

2006

Preprint:

This is an accepted article published in International Journal of Heat and Mass Transfer. The final authenticated version is available online at:
[https://doi.org/\[DOI not available\]](https://doi.org/[DOI not available])



ELSEVIER

Available online at www.sciencedirect.com

SCIENCE @ DIRECT®

International Journal of Heat and Mass Transfer xxx (2005) xxx–xxx

International Journal of
HEAT and MASS
TRANSFER

www.elsevier.com/locate/ijhmt

Optimization of micro heat exchanger: CFD, analytical approach and multi-objective evolutionary algorithms

Kwasi Foli ^{a,1}, Tatsuya Okabe ^b, Markus Olhofer ^b, Yaochu Jin ^b, Bernhard Sendhoff ^{b,*}

^a Honda Research Institute USA Inc., 1381 Kinnear Road, Columbus, OH 43212, USA

^b Honda Research Institute Europe GmbH, Carl-Legien-Strasse 30, D-63073 Offenbach/M, Germany

Received 12 April 2005; received in revised form 8 August 2005

Abstract

Advances in miniaturization have led to the use of microchannels as heat sinks in industry. Studies have established that the thermal performance of a microchannel depends on its geometric parameters and flow conditions. This paper describes two approaches for determining the optimal geometric parameters of the microchannels in micro heat exchangers. One approach combines CFD analysis with an analytical method of calculating the optimal geometric parameters of micro heat exchangers. The second approach involves the usage of multi-objective genetic algorithms in combination with CFD.

© 2005 Published by Elsevier Ltd.

Keywords: Computational fluid dynamics; Micro heat exchanger; Optimization; Multi-objective; Optimal shape; Evolutionary algorithms

1. Introduction

The trend toward miniaturization and the advances in microfabrication have led to the application of microchannels for thermal management in areas such as medicine, consumer electronics, avionics, metrology, robotics, process industry, telecommunication and automotive industries to mention just a few. Since the work of Tuckerman and Pease [1], microchannels have received considerable attention particularly in the areas of experimental [2–10], analytical [11–19] and numerical [10,20–23] studies. These studies revealed deviations in the heat transfer and fluid flow characteristics in microscale devices from those of conventionally-sized (or macro-scale) devices. The flow and heat transfer characteristics of fluids flowing in microchannels could not be adequately predicted by the theories

and correlations developed for conventionally-sized channels. The studies [15,16] further showed that the performance of a microchannel heat exchanger depends very much on the aspect ratio (AR) of the channels. Bau [24] conducted optimization studies to minimize temperature gradient and overall thermal resistance in microchannels and concluded that reduction in overall thermal resistance could be achieved by varying the cross-sectional dimensions of a microchannel.

In spite of the widespread use of micro heat exchangers (μ HEXs) in the process and automotive industries, there is limited published literature on attempts at designing them for optimal performance.

The objective of this paper is to present two methods for determining the optimal design parameters of the microchannels in μ HEXs that maximize the heat transfer rate (or heat flux) subject to specified design constraints. The first is a simple approach that combines CFD with the analytical solution of a simplified transport equation for momentum and heat transfer. This approach optimizes the dimensions of a microchannel with predetermined geometry. The second approach, a more sophisticated

* Corresponding author.

E-mail addresses: Kwasi.Foli@SARTORIUS.com (K. Foli), tatsuya_okabe@n.w.rd.honda.co.jp (T. Okabe), bs@honda-ri.de (B. Sendhoff).

¹ Present address: Sartorius AG, Weender Landstrasse 94-108, D-37075 Göttingen, Germany.

Nomenclature

| | |
|--|---|
| b | length scale as defined in Eq. (5) |
| c_p | specific heat capacity at constant pressure |
| d_h | hydraulic diameter |
| g | acceleration due to gravity |
| h | heat transfer coefficient, specific enthalpy (in Eq. (3)) |
| H | height of microchannels |
| k | thermal conductivity |
| l | length of channel |
| Nu | Nusselt number |
| u_i | velocity component in tensor notation |
| p | pressure |
| ΔP (ΔP_h , ΔP_c) | pressure drop (hot, cold gas channel) |
| s | thickness of material separating channels (Table 2) |
| T | temperature |

| | |
|-------|------------------------------|
| x_i | general coordinate direction |
| w | width of channel |
| Q | heat transfer |

Greek symbols

| | |
|---------------|--------------------------|
| α | ratio in Eq. (7) |
| β | bulk viscosity |
| δ_{ij} | Kronecker delta function |
| μ | dynamic viscosity |
| ρ | density |
| τ_{ij} | stress tensor |

Subscripts

| | |
|---|---------|
| c | channel |
| f | fluid |
| s | solid |

55 method, not only determines the optimal dimensions of a
56 heat exchanger but also determines the optimum shape
57 based on imposed operating conditions. This approach in-
58 creases the degree of freedom of the geometrical variations
59 by combining CFD analyzes with multi-objective evolu-
60 tionary algorithms (MOEAs).

61 2. Mathematical model

62 The problem under consideration is the forced convec-
63 tion through μ HEX. A schematic model of the μ HEX is
64 shown in Fig. 1. It consists of rectangular channels with
65 hot and cold fluid flowing through alternate channels.
66 The dimensions of the heat exchanger core are shown in

the figure. The method described here applies to both co- 67
and counter-flow configurations. 68

For the studies reported in this paper, the hydraulic 69
diameter of microchannels considered was between 70
100 μm and 1000 μm . The Knudsen number for all the 71
flows considered was less than 0.001, a necessary condition 72
for continuum flow. Therefore, the conservation equations 73
based on continuum flow apply. The governing equations 74
that describe the steady state momentum and heat are gi- 75
ven in tensor notations below. 76

Continuity and momentum 77

$$\frac{\partial}{\partial x_i}(\rho v_i) = 0, \quad \rho u_j \frac{\partial u_i}{\partial x_j} = -\frac{\partial p}{\partial x_i} + \rho g_i + \frac{\partial \tau_{ij}}{\partial x_j}, \quad \text{where} \quad (1) \quad 79$$

$$\tau_{ij} = \mu \left(\frac{\partial u_i}{\partial x_j} + \frac{\partial u_j}{\partial x_i} \right) + \left(\beta - \frac{2}{3} \mu \right) \frac{\partial u_k}{\partial x_k} \delta_{ij}. \quad 79$$

Energy 80

$$\rho u_j \frac{\partial h}{\partial x_i} = u_i \frac{\partial p}{\partial x_i} + \phi + \frac{\partial}{\partial x_i} \left(k \frac{\partial T}{\partial x_i} \right), \quad \text{where } \phi = \tau_{ij} \frac{\partial u_i}{\partial x_j}. \quad (2) \quad 82$$

In steady state the conservation equations are written in the 83
general form 84

$$\frac{\partial}{\partial x_i}(\rho u_i \phi) = \frac{\partial}{\partial x_i} \left(\Gamma \frac{\partial \phi}{\partial x_i} \right) + S, \quad (3) \quad 85$$

where ϕ represents a general dependent variable such as 88
velocity or temperature, Γ is a diffusion coefficient and S 89
is a source term. The partial differential equations repre- 90
sented in general by Eq. (3) were discretized over spatial 91
coordinates by means of the control volume technique 92
[25]. To predict the thermal performance of the μ HEX 93
the resulting finite difference equations were solved in 94
three-dimensions using an iterative, segregated solution 95

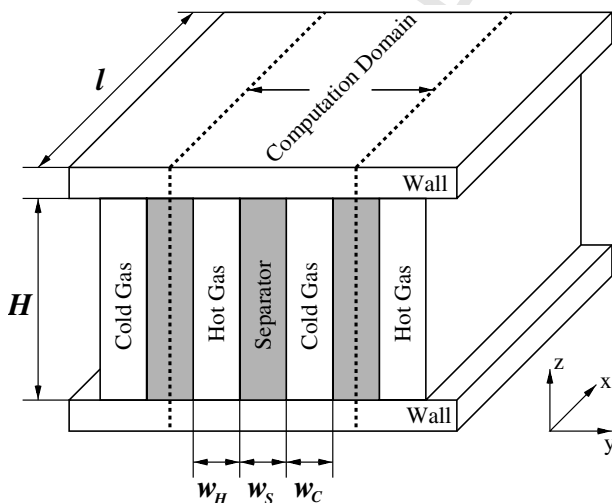


Fig. 1. A schematic model of the micro heat exchanger. The micro heat exchanger consists of three parts, i.e., a hot gas channel, a cold gas channel and a separator. The heat energy in the hot gas channel will be transferred to the cold gas channel via the separator.

96 method wherein the equation sets for each dependent variable were solved sequentially till a preset convergence criterion was satisfied. The SIMPLEC solution algorithm [26] was used to treat the pressure–velocity coupling of the flow field. To ensure faster convergence of the equations, an Algebraic Multigrid solver [27] was used for each of the resulting algebraic finite difference equations. The set of equations were solved using a commercial CFD software, CFD-ACE+ [28] that incorporates the aforementioned equation solver and solution strategy. In solving the transport equations, the Dirichlet boundary conditions were set for the mass flow rate and temperature of the fluids at the inlet boundaries, while the Neumann boundary conditions were specified for the temperature and velocity components at the outlet boundaries of the computational domains. Adiabatic boundary conditions were imposed on the walls and the continuity of the temperature and heat flux was used as the conjugate boundary conditions to couple the energy equations for the solid and fluid phases. The no-slip boundary condition was imposed on the velocity components at the wall. Finally, the ideal-gas law was used to calculate the thermodynamics properties of the gases used in the study. Since geometric periodicity exists in the cases studied exists the computational domain is simplified as shown marked in Fig. 1.

121 In performing the simulation the computational domain was populated with structured (hexahedral) cells. For each study, a grid-independent solution was achieved and the number of cells depended on the aspect ratio that was investigated. Typically, a grid-independent solution was achieved for the lower aspect ratio cases with about 43,500 cells. With a convergence criterion set at 0.0001, convergence was attained at an average time of 1440 CPU seconds.

130 3. Optimization

131 3.1. Analytical approach combined with CFD

132 The optimal geometric parameters of the channels of a μ HEX are determined using a combination of CFD and the analytical approach of Samalam [12]. Samalam reduced the analysis of the microchannel flow problem to a quasi two-dimensional differential equation and presented exact solutions to analytically determine the optimal dimensions of microchannels under given constraints. Based on the given constraints such as pumping power and space limitation the variables to be optimized are the channel width, aspect ratio and channel spacing. The optimal aspect ratio of the μ HEX channels, subject to the constraints imposed, was determined using CFD. As would be explained later, based on the problem specification, the optimal geometric parameters of a microchannel are either directly obtained based on the determined optimal aspect ratio or these are calculated by combining the optimal aspect ratio with the relationships derived by Samalam.

The first step towards the optimization was to determine the performance characteristics of the μ HEX by numerically solving the conservation equations. The two design scenarios considered were: (1) the allowable volume of the heat exchanger was fixed based on design constraints; (2) no limit was placed on the volume of the μ HEX core. However, the dimensions of the microchannels were within the limits defined for a μ HEX. For both cases, Inconel with a thickness of 0.1 mm was the material of the μ HEX; nitrogen was used as the hot fluid and carbon dioxide as the coolant.

3.1.1. Determination of the optimal aspect ratio for constant volume of microchannels

This situation applies to cases where the volume of the μ HEX is fixed by design considerations. In the study presented in this paper, each microchannel of the heat exchanger was assigned a volume of 50 mm³. Assuming a fixed length of 40 mm for all channels, this resulted in a constant cross-sectional area of 1.25 mm² for each microchannel. For the analysis, the aspect ratio, AR, of a channel, was defined as the ratio of height of channel to its width, i.e.,

$$AR = \frac{H}{w_c} \quad (4)$$

Numerical simulations were performed by varying the aspect ratio of the microchannels in the range $1.25 \leq AR \leq 86.8$ whilst maintaining a constant cross-sectional area, in this case, of 1.25 mm². For a constant cross-sectional area of channel, the aspect ratio was varied by varying both the width w_c , and height H , of the channels. For the simulation, 10^{-5} kg/s per channel of N₂ at 1.358 bar and 750 °C and 10^{-5} kg/s per channel of CO₂ at 1.338 bar and 220 °C in counter-flow were the working fluids.

Fig. 2 shows the variation of heat flux, heat transfer rate and pressure drop in each channel with the aspect ratio, AR. It is clear from the figure that as the aspect ratio of the microchannel increases there is a rapid decrease in the heat flux coupled to a rapid increase in the pressure drop. Since the heat flux, and for that matter the heat transfer coefficient, and pressure loss have opposing trends there must be a balance between the two in choosing an optimal aspect ratio. The optimal aspect ratio lies in the optimal region which is the region between the intersection of the tangents at the points of maximum and minimum curvature on the heat transfer rate and heat flux curves. This region, marked by the ellipse shown in Fig. 2, corresponds to the projection of the points *A* and *B* onto the abscissa, i.e., *A'* and *B'*. To the left of that region, even though the heat flux is high and pressure loss is low in the μ HEX, by its very design (see Fig. 1), the heat transfer rate is low. On the other hand, the portion of the graph to the right of the optimal region shows a very gradual increase in heat transfer with a correspondingly high pressure loss. It stands to reason that not much would be gained in designing the heat exchanger to operate in that zone (to the

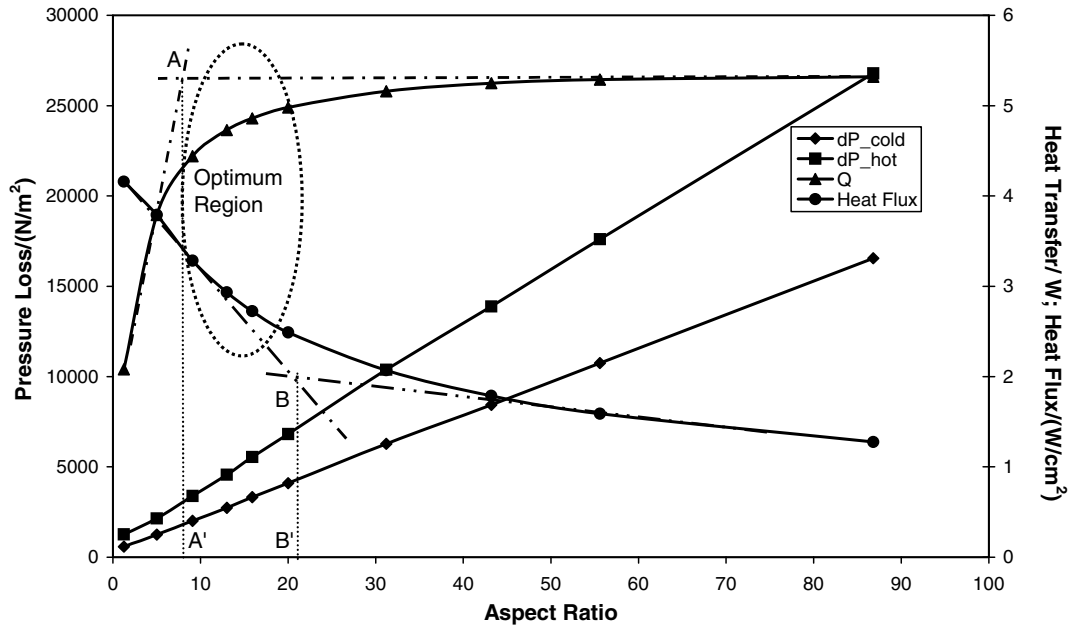


Fig. 2. Variation of pressure loss, heat transfer rate and heat flux with channel aspect ratio (constant volume).

right of the optimum region). It follows from the above discussion that for a given material and volume of μ HEX, the optimal dimensions of the channels could be obtained based on the choice of optimal aspect ratio which must lie within $A'B'$.

Below are examples of the microchannel dimensions based on aspect ratios within the marked optimum region are shown:

- (1) Optimal height = 3.38 mm, optimal width = 0.37 mm, AR = 9.1,
- (2) Optimal height = 4.03 mm, optimal width = 0.31 mm, AR = 13.0,
- (3) Optimal height = 4.46 mm, optimal width = 0.28 mm, AR = 15.9,
- (4) Optimal height = 5.00 mm, optimal width = 0.25 mm, AR = 20.0.

3.1.2. Variable volume of microchannels

In this study, the volume of the μ HEX varied but was kept within limits that define a μ HEX (i.e., $1 \mu\text{m} \leq d_h \leq 1000 \mu\text{m}$). The flow rate of fluid (hot and cold) was kept constant for the different volume of μ HEXs analyzed. Similar to Section 3.1.1 the length of the microchannels was fixed leaving the cross-sectional area as the variable. For the sake of simplicity the aspect ratio was varied by changing the height of microchannels but keeping the width constant at 0.25 mm. CFD simulations were performed by varying the aspect ratio of the microchannels in the range $5 \leq \text{AR} \leq 100$. For the analysis, 1.12×10^{-5} kg/s per channel of N_2 at 1 bar and 750°C and 6.0×10^{-6} kg/s per channel of CO_2 at 1 bar and 220°C in counter-flow were used as working fluids.

Fig. 3 shows the variation of heat flux, heat transfer rate and pressure drop in each channel with the aspect ratio, AR. As the aspect ratio of the microchannel increases there is a corresponding increase in the heat transfer rate up to a maximum value after which the heat transfer rate decreases. For constant mass flow rate of fluid, a higher aspect ratio leads to lower fluid velocity. In addition, the hydraulic diameter of the channel increases with aspect ratio. The increase in hydraulic diameter with aspect ratio combined with the attendant decrease in fluid velocity leads to lower pressure drop in the channels as is shown in the figure.

For the geometry under consideration (Fig. 1), increasing the channel aspect ratio increases the heat transfer area and consequently the transfer of heat. On the other hand, the increase in aspect ratio reduces the fluid velocity (and consequently the Reynolds number of the flow) thus leading to a lower heat transfer coefficient. Thus, there are two competing factors contributing to the transfer of heat. A point is reached when the gain in heat transfer with increasing aspect ratio is offset by the loss caused by the decrease in convective heat transfer coefficient as a result of the lower velocity and hence the Reynolds number. This effect is reflected in the curve of the heat transfer rate, Fig. 3.

The broken line in Fig. 3 marks the (optimal) aspect ratio corresponding to the maximum heat transfer rate. The portion of the figure to the left of the maximum is characterized by high heat flux as well as high pressure loss. On the other hand, the portion to the right of the optimal aspect ratio shows a very gradual decrease in heat transfer whereas the aspect ratio and hence the volume of μ HEX increases. Thus, operating in the region to the right of the maximum point would tremendously reduce the energy density of a μ HEX.

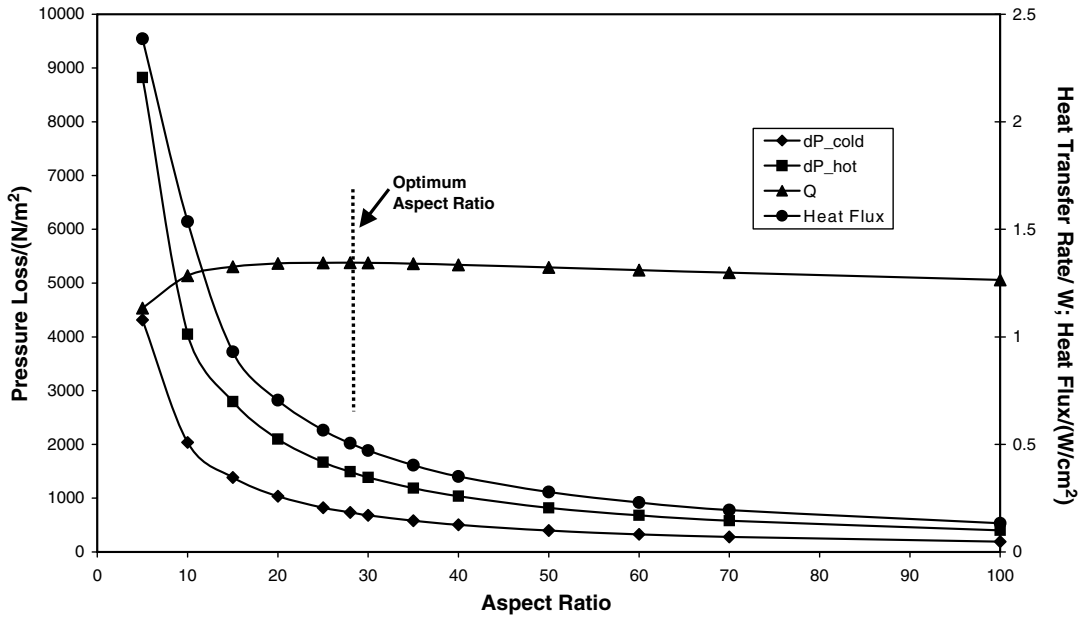


Fig. 3. Variation of pressure loss, heat transfer rate and heat flux with channel aspect ratio (variable volume).

271 It must be emphasized that the graphs shown in Figs. 2
 272 and 3 are case-specific and the designer of a μ HEX must
 273 first obtain the characteristic curves for the type of heat ex-
 274 changer under consideration. Based on the characteristics
 275 and the design constraints an optimal AR and, subse-
 276 quently, the optimal dimensions could be obtained.

277 3.1.3. Optimal dimensions

278 This section deals with the approach used in calculating
 279 the optimal geometric parameters of the channels of a
 280 μ HEX when the volume of the μ HEX is not fixed by design
 281 considerations (Section 3.1.2). Associated with any known
 282 optimal aspect ratio, AR_{opt} , is an infinite number of pairs
 283 of channel height and width.

284 In calculating the optimal dimensions of the microchan-
 285 nel based on the chosen AR the analytical approach of
 286 Samalam [12] was used. Though derived for microchannels
 287 designed for cooling electronic chips, a thorough investiga-
 288 tion of the analysis revealed that the approach could be ap-
 289 plied to the type of μ HEXs discussed here.

290 According to Samalam, for low aspect ratios, $AR \leq 10$,
 291 the optimal dimensions of a microchannel are given by
 292

$$294 \quad w_c = b, \quad \text{and} \quad w_s = H \sqrt{\frac{k_f Nu}{6k_s}}, \quad \text{where} \quad b^4 = \frac{12\mu k_f Nu l^2}{\rho c_p \Delta P}. \quad (5)$$

295 The above is valid for

$$296 \quad \frac{H}{b} \ll \pi^2 \left[\frac{k_s}{6k_f Nu} \right]^{1/2}. \quad (6)$$

299 For high aspect ratios, $AR > 10$

$$300 \quad w_s = \frac{w_c}{2}, \quad \text{and} \quad w_c = \frac{2^{1/6} b^{4/3}}{\alpha^{1/6} H^{1/3}}, \quad \text{where} \quad \alpha = \frac{k_f Nu}{k_s}. \quad (7)$$

Eq. (7) are valid for

$$\frac{H}{b} \gg \frac{\pi^{3/4}}{(2\alpha)^{1/4}}. \quad (8)$$

307 The steps followed for calculating the optimal geometric
 308 parameters are discussed in Table 1. Since optimal geomet-
 309 ric parameters are dependent on the thermophysical prop-
 310 erties of fluids, it is obvious that a μ HEX exchanger
 311 operating with two different fluids or even with the same
 312 fluid at different temperatures will have different optimal
 313 dimensions for the channels transporting both fluids.

314 For the purpose of illustration the optimal geometrical
 315 parameters of a μ HEX based on the operating conditions
 316 provided in this subsection are calculated. In Fig. 3, the
 317 optimal aspect ratio, AR_{opt} , corresponding to the maxi-
 318 mum heat transfer rate is 28. The task of determining the

Table 1
Optimization steps

| $AR_{opt} \leq 10$ | $AR_{opt} > 10$ |
|---|---|
| Determine Nu based on fluid properties | Determine Nu based on fluid properties |
| Fix allowable pressure loss ΔP | Fix allowable pressure loss ΔP |
| Decide on length of channels, l based on space limitation | Decide on length of channels, l based on space limitation |
| Calculate b from Eq. (5) | Calculate b from Eq. (5) |
| From Eq. (5), $w_c = b$ | Calculate α form Eq. (7) |
| From Eq. (4), $H = w_c AR_{opt}$ | From Eqs. (4) and (7), $w_c = \frac{2^{1/8} b}{\alpha^{1/8} AR_{opt}^{1/4}}$ |
| From Eq. (5), $w_s = w_c AR_{opt} \sqrt{\frac{k_f Nu}{6k_s}}$ | From Eq. (4), $H = w_c AR_{opt}$ |
| Check the validity condition (Eq. (6)) | From Eq. (7), $w_s = \frac{w_c}{2}$ |
| | Check the validity condition (Eq. (8)) |

319 optimal dimensions from the infinite set of all possible
 320 pairs, (H, w_c) , is accomplished by using Eq. (7) (for
 321 $AR_{opt} > 10$). Using average values based on inlet and out-
 322 let temperatures for the fluid properties appearing in Eqs.
 323 (5)–(8), the dimensions of the hot and cold side channels
 324 were calculated as follows:

Hot side: $H = 14.80$ mm, $w = 0.53$ mm, $s = 0.26$ mm,

Cold side: $H = 11.76$ mm, $w = 0.42$ mm, $s = 0.21$ mm.

326

327 For the geometry under consideration it would not be fea-
 328 sible from a design point to have different dimensions for
 329 the hot- and cold-side microchannels. Further numerical
 330 simulations revealed that better results were achieved when
 331 the cold-side dimensions were used for all channels.

332 The performance of three μ HEXs having the same as-
 333 pect ratio was compared with a μ HEX optimized according
 334 to the procedure described in this section. In Table 2 the
 335 dimensions, heat transfer rate and pressure loss in all four
 336 μ HEXs are provided. A close examination of the results
 337 puts the performance of the optimized μ HEX above the
 338 pack.

339 3.2. Optimization with multiple criteria

340 In μ HEXs there are several usually competing properties
 341 that must be taken into account, e.g., the minimization of
 342 the pressure drop and the maximization of the heat flux.
 343 In the second approach, we will, therefore, treat the design
 344 of μ HEX as a multi-objective optimization problem. Here,
 345 the target is a set of solutions called the Pareto front of a
 346 multi-objective optimization (MOO) problem. The defini-
 347 tion of the Pareto front will be provided in Section 3.2.1.
 348 To tackle MOO problems, we will use evolutionary algo-
 349 rithms. Besides the known strength of evolutionary compu-
 350 tation, like robustness and the possibility to escape local
 351 optima, the population based approach of evolutionary
 352 methods is particularly suitable for MOO problems be-
 353 cause the target is to identify a set of solutions instead of
 354 one optimal solution.

355 3.2.1. Evolutionary multi-objective optimization

356 In this section, we will shortly introduce the main prin-
 357 ciples of evolutionary algorithms and outline the multi-
 358 objective optimization method [29,30].

359 Evolutionary algorithms (EAs) are direct pseudo-sto-
 360 chastic search methods which mimic the principles of
 361 Neo-Darwinian evolution. A population of possible solu-
 362 tions (e.g., a vector² of continuous parameters, the objec-
 363 tive variables, describing a μ HEX geometry) is adapted
 364 to solve a given problem (e.g., minimization of pressure
 365 drop) over several generations. The adaptation occurs by
 366 varying these solutions in the population and by selecting
 367 the best solutions for the next generation. The variations

Table 2

Comparison between optimized and non-optimized μ HEXs

| | H (mm) | w (mm) | s (mm) | AR | Q (W) | ΔP_{cold} (Pa) | ΔP_{hot} (Pa) |
|------------------|-------------|-------------|-------------|----|------------|---------------------------|--------------------------|
| Optimized HEX | 11.76 | 0.42 | 0.21 | 28 | 3.59 | 446 | 1333 |
| HEX1 | 5.88 | 0.21 | 0.105 | 28 | 0.790 | 1503.0 | 5132 |
| HEX2 | 7.84 | 0.28 | 0.140 | 28 | 0.747 | 425.0 | 1565 |
| HEX3 | 12.88 | 0.46 | 0.231 | 28 | 0.752 | 57.55 | 210 |

can be classified as purely stochastic (usually called muta- 368
 tion) and combinatoric/stochastic (usually called recombini- 369
 tion or in the context of genetic algorithms crossover). 370
 Schematically the evolution cycle is shown in Fig. 4(a), for- 371
 mally, an evolutionary algorithm can be described by 372
 Fig. 4(b). 373

In multi-objective optimization, several competing 374
 objectives exist. As discussed in Section 3.1, this is the case 375
 for μ HEX optimization. There are different ways to deal 376
 with MOO problems. One can aggregate (mostly linearly) 377
 all objectives and render the problem single objective. 378
 The drawback of this approach is that the choice of the 379
 weights is usually arbitrary. Alternatively, one can deter- 380
 mine all solutions for which no solutions exist which are 381
 better in all objectives. These solutions are called *non-dom-* 382
inated and the set of all non-dominated solutions is referred 383
 to as the *Pareto front*, see Fig. 5. 384

The second approach leaves maximum freedom to the 385
 designer since objectives are not weighted prior to the opti- 386
 mization but instead the most appropriate solution is cho- 387
 sen from the Pareto front. However, it is also the 388
 computationally most demanding approach considered in 389
 this work. Since EAs inherently operate on a set of solu- 390
 tions, the so-called *population*, they are particularly suitable 391
 to find and represent the Pareto front. 392

In this paper, we will apply the NSGA-II [31,32] to iden- 393
 tify the Pareto front, which is widely recognized as one of 394
 the most powerful MOO algorithms. The Pareto front for 395
 the NSGA-II is represented in the final population. 396

The NSGA-II (a fast and elitist non-dominated sorting 397
 genetic algorithm) proposed by Deb et al. [31,32] is a 398
 multi-objective extension of the standard genetic algorithm 399
 with binary/gray coding. In the context of NSGA-II, a 400
 floating point representation can also be used. Whether a 401
 binary/gray coding is more or less suitable than a floating 402
 point representation is especially for multi-objective opti- 403
 mization difficult to decide and certainly depends on the 404
 problem. Some preliminary research indicates that the best 405
 choice would be a hybrid representation, so that a switch- 406
 ing mechanism is able to choose the current optimal repre- 407
 sentation dependent on the search space, see [33]. 408

In our approach, the real parameter values are binary 409
 encoded and the standard crossover and mutation method 410
 are used for the variation of solutions. The selection meth- 411
 od is based on two measures which are specific to MOO. 412
 The above introduced principle of non-domination is used 413
 as well as a measure that aims at maintaining diversity and 414

² Note, that this vector is also called chromosome in imitation of evolutionary biology.

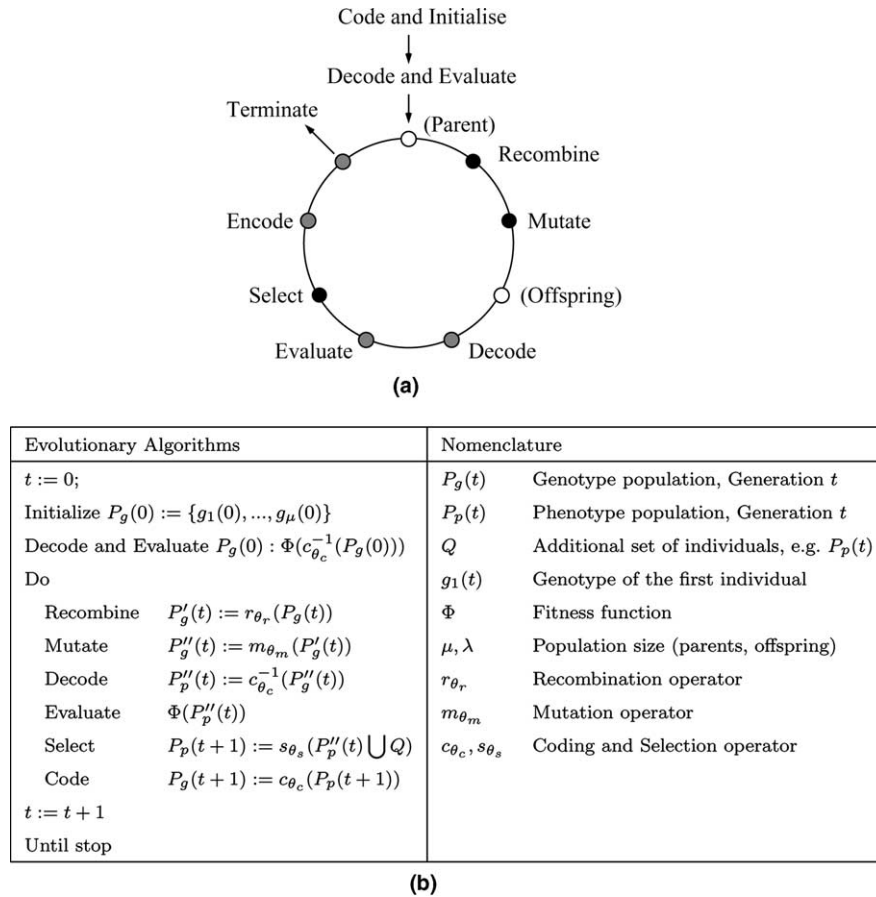


Fig. 4. Flow of evolutionary computation. First, a population is generated randomly and evaluated. This becomes the parent population, from which offspring are generated using recombination (crossover) and mutation. From the evaluated offspring population, promising individuals are selected to become the next parent population. This iteration is repeated until a certain termination condition is met. (a) Evolution cycle, (b) formal description of evolutionary algorithms.

415 “spread” of the solutions that are to represent the Pareto
416 front. Details of the algorithm can be found in [31,32].

417 3.2.2. Optimization environment

418 3.2.2.1. Design parameters. The goal is to find the optimal
419 shape of the separator that simultaneously maximizes heat
420 transfer and minimizes pressure drop in the micro heat ex-
421 changer. To simplify this problem, the height H and the
422 length l in Fig. 1 are fixed. In addition, the cross-sectional
423 area of the flow passages are also kept constant. The shape
424 of the separator is represented by two *Non-Uniform Ra-*
425 *tional B-splines (NURBS)* [34]. The *B-spline* representation
426 consists of a number of control points, which define the
427 control polygon of the shape, a number of knot points and
428 a number of weights. We keep the knot points and
429 the weights³ constant and only vary the control points.
430 In this work, we use 10 control points. We specify one
431 end wall of the separator with the spline and define the sec-
432 ond wall using the constant thickness of the separator.⁴

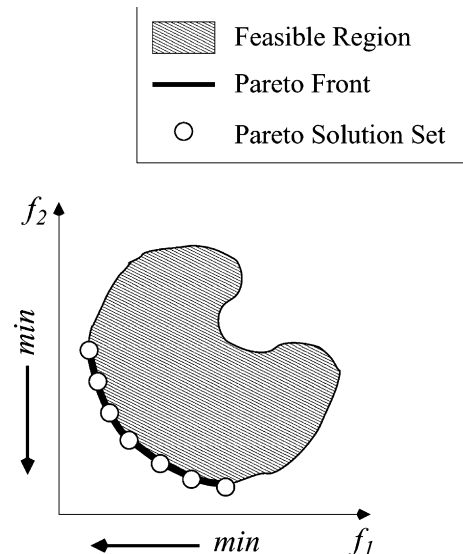


Fig. 5. Pareto front and Pareto solution set. Here, two objectives to be minimized are assumed. The bold curve is the Pareto front that is the solution of multi-objective optimization.

³ The weights are set to one.

⁴ To keep the cross-sectional area of the flow passages constant, their width are modified according to the shape of the separators.

3.2.2.2. *Objective functions.* The objectives of the optimization are to maximize the heat transfer and to minimize the pressure drop in the hot gas channel and in the cold gas channel [35,36]. To render both problems minimization problems, we multiply the heat transfer by -1 . Therefore, we get the following two objectives:

$$f_1(\vec{x}) = -Q, \quad f_2(\vec{x}) = \Delta P_h + \Delta P_c, \quad (9)$$

where Q is the heat transfer and ΔP_h and ΔP_c are the pressure drops in the hot gas channel and in the cold gas channel, respectively.

3.2.2.3. *Calculation constraints and mesh generation.* The hot gas consists of a mixture of methane, hydrogen, steam, carbon monoxide, carbon dioxide and nitrogen; the cold gas is a mixture of methane, steam, oxygen and nitrogen.

The heat transfer with the surroundings is assumed adiabatic. In this problem the exchange of heat between alternate channels is across the separator.

The inlet conditions for the gases are as follows:

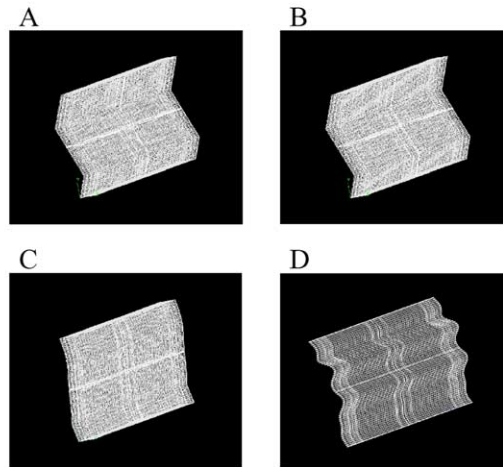
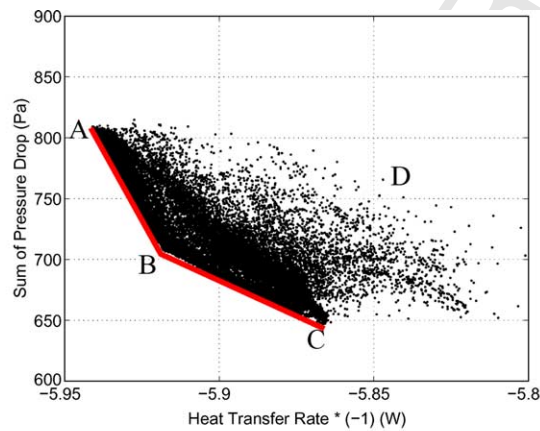
Flow rate (g/s) = 3.06 (for hot gas and cold gas),

Inlet temperature ($^{\circ}\text{C}$) = 750, 220 (for hot gas, cold gas),

Inlet pressure (kPa gauge) = 34.5, 36.5 (for hot gas, cold gas),

Allowable pressure drop (kPa) = 1.0 (for hot gas and cold gas).

For the optimization the CFD-ACE+ program had to be interfaced with the multi-objective evolutionary algorithms. The details of this interface are explained in [35,36].



| Point | HTR(W) | $\Delta P_h(\text{Pa})$ | $\Delta P_c(\text{Pa})$ | Heat Flux ($10^{-8}\text{W}/\text{m}^2$) |
|-------|--------|-------------------------|-------------------------|--|
| A | 5.941 | 458.6 | 350.4 | 1.106 |
| B | 5.918 | 386.6 | 321.1 | 1.101 |
| C | 5.866 | 357.5 | 289.4 | 1.161 |
| D | 5.840 | 431.6 | 343.1 | 1.031 |

Fig. 6. Final result by NSGA-II (after one-month calculation). In the upper figure, all evaluated individuals are shown. One point corresponds to one design of μHEX . The gray (red in the web version) line (AB, CD) shows the estimated Pareto curve. Four representative shapes A, B, C and D are shown together with their values for heat transfer rate (HTR), pressure drops ΔP_h , ΔP_c and the heat flux.

462 The auto-mesh generator for a structural grid from
 463 CFD-ACE+ was used in the optimization. In order to han-
 464 dle poorly generated meshes or errors in the spline repre-
 465 sentation (e.g., loops), individuals for which the flow
 466 solver was unable to satisfy a preset convergence criterion
 467 were removed from the population.

468 3.2.3. Results of NSGA-II

469 The parameters in NSGA-II are set as follows:

Number of individuals = 100,
 Number of bits per one floating value = 20,
 Range of floating value in Y -direction = $[-0.25H, 0.25H]$
 (accuracy = $0.5H \times 2^{-20} \approx 0.5H \times 10^{-6}$),
 Range of floating value in Z -direction = $[0, H]$
 (accuracy = $H \times 2^{-20} \approx H \times 10^{-6}$),
 Maximum generations = 500,
 Crossover/rate = One point crossover/0.9,
 Mutation/rate = Bit flip/0.05.

479 The result of the optimization study is shown in Fig. 6 with
 480 each point representing a solution. The figure shows all
 481 evaluated solutions and the estimated Pareto curve as red
 482 (gray) lines. The shapes of three representative solutions
 483 (together with their values for heat transfer rate (HTR),
 484 pressure drops ΔP_h , ΔP_c and heat flux) on the Pareto front
 485 and one solution far away from the Pareto front are shown.
 486 The results clearly reveal the conflict between the two
 487 objectives, the heat transfer and the pressure drop. Any
 488 geometrical change that increases the heat transfer rate
 489 and for that matter the heat flux leads to an increase in
 490 the pressure drop and vice versa. Thus, it is evident that
 491 multi-objective optimization techniques are necessary for
 492 the optimization of the μ HEX. We also observe that the
 493 Pareto front consists of two parts, i.e., the lines \overline{AB} and
 494 \overline{BC} . One would expect that the shapes of the μ HEX on
 495 both parts are different, however they are not. The reason
 496 for the bend in the Pareto front at point B remains unclear
 497 and will be the subject of further studies.

498 All shapes on the Pareto front are (at least topologically,
 499 e.g., with regard to their periodicity⁵) strikingly similar.
 500 Theoretically, the spline with 10 control points can repre-
 501 sent curves with higher periodicity than the ones obtained.
 502 A natural question is why all geometries that are visited by
 503 the optimization algorithm have relatively similar shape
 504 and low periodicity. Although the data obtained from
 505 our experiments is not sufficient to give a definite answer
 506 to this question, we can offer two hypotheses: (1) although
 507 theoretically possible, the practical realization of shapes
 508 with higher periodicity by splines with 10 control points
 509 is difficult and requires correlated changes of the control

points which are difficult to achieve for stochastic optimi- 510
 zation methods like evolutionary algorithms; (2) the ratio 511
 of the number of geometries with good performance to 512
 all geometries becomes smaller with increasing periodicity, 513
 i.e., even though higher periodicity might lead to better 514
 solutions, they are harder to find. There is some evidence 515
 for both suggestions. In particular, the first one seems intu- 516
 itively correct, although for a robust optimization tech- 517
 nique it should still be possible to realize splines with 518
 higher periodicity. The fact that in Fig. 6, a poorly per- 519
 forming solution (D) has a shape with higher periodicity 520
 might point in the direction of the second hypothesis. Some 521
 first results with a different representation have been ob- 522
 tained in [35]. A combination of both representations 523
 might allow to answer the question on the influence of 524
 the representation on the optimization result more 525
 comprehensively. 526

527 4. Conclusion

It has been demonstrated in this paper that the perfor- 528
 mance of micro heat exchangers depends on the operating 529
 conditions and aspect ratio of the microchannels that make 530
 up the flow passages. Using the simpler approach we were 531
 able to optimize the dimensions of a rectangular micro- 532
 channel. The optimized dimensions presented in Section 533
 3.1.3 lead to higher heat flux and heat transfer rates. 534

With the more advanced approach, we discussed the 535
 problem of the optimal shape of micro heat exchangers 536
 in the context of multi-objective evolutionary optimization. 537
 Here we introduced two objectives, the heat transfer and 538
 the sum of pressure drops. We applied NSGA-II (Non- 539
 dominated Sorting Genetic Algorithm) to identify the Pare- 540
 to front that is the trade-off curve between the two objec- 541
 tives for this problem. Starting with a rectangular shape, 542
 our optimization tool was able to generate different geom- 543
 etries. The optimum geometry obtained with this method 544
 yielded heat fluxes greater than those obtained with the less 545
 advanced approach. 546

There are several conclusions which can be drawn from 547
 our studies: 548

- The performance of micro heat exchangers with respect 549
 to the measures that we analyzed in this paper clearly 550
 depends on their geometry. 551
- There is a trade-off between minimal pressure drop and 552
 maximal heat transfer. This trade-off is made visible by 553
 the Pareto curves that we obtained in our optimization 554
 experiments. 555
- The dependence of the performance on the geometry is 556
 non-trivial, i.e., simply increasing the periodicity does 557
 not necessarily lead to better solutions. 558

Results that have been published previously in the liter- 559
 ature gave higher heat flux values than those obtained in 560
 this paper. Higher heat flux and heat rate values could be 561
 easily obtained by changing the operating conditions and 562
 563

⁵ We use the term periodicity in a rather intuitive way. Mathematically, a function $w(t)$ is periodic, if $w(t) = w(t + T)$ with the period $T = v^{-1}$ and frequency v . Higher periodicity here implies higher frequency. However, in our intuitive use of periodicity, we describe end walls which are similar to e.g., a sine or a saw-tooth pattern with long or short period.

564 the type of fluid. However, the target of this paper is to
 565 analyze the intrinsic interaction between performance and
 566 design or shape of micro heat exchangers on the back-
 567 ground of different optimization techniques. Pareto curves
 568 of the optimization exhibit some interesting dependencies.
 569 It will be the target of future work to confirm these depen-
 570 dencies by real experiments and to get a more in-depth
 571 understanding of the relation between the periodicity of
 572 the geometry and the performance of the micro heat ex-
 573 changer both with respect to minimal pressure drop and
 574 maximal heat transfer.

575 Acknowledgements

576 The authors would like to thank E. Körner, A. Richter,
 577 L. Freund and T. Arima for their kind and continuous sup-
 578 port. Mr. Peters of CFD Research Corporation is acknowl-
 579 edged for his flexibility regarding the parallel interface
 580 between CFD-ACE+ and our optimization software. We
 581 also thank K. Shibata (Wave Front Co., Ltd.) for his sup-
 582 port to build up the connection between the CFD part and
 583 the optimization.

584 References

585 [1] D.B. Tuckerman, R.F.W. Pease, High-performance heat sinking for
 586 VSLI, *IEEE Electron Dev.* 2 (1981) 126–129.
 587 [2] J. Pfahler, J. Harley, H.H. Bau, J. Zemel, Liquid and gas transport in
 588 small channels, in: D. Choi et al. (Ed.), *ASME-DSC 19*, 1990, pp.
 589 149–157.
 590 [3] J. Pfahler, J. Harley, H.H. Bau, J. Zemel, Gas and liquid flow in small
 591 channels, in: D. Choi et al. (Ed.), *Micromechanical Sensors, Actu-*
 592 *ators and Systems*, ASME-DSC 32, 1991, pp. 49–60.
 593 [4] X.F. Peng, G.P. Peterson, B.X. Wang, Frictional flow characteristics
 594 of water flowing through rectangular microchannels, *Exp. Heat*
 595 *Transfer* 7 (1994) 249–264.
 596 [5] X.F. Peng, G.P. Peterson, The effect of thermo-fluid and geometrical
 597 parameters on convection of liquids through rectangular channels,
 598 *Int. J. Heat Mass Transfer* 38 (4) (1995) 755–758.
 599 [6] X.F. Peng, G.P. Peterson, Convective heat transfer and flow friction
 600 for water flow in microchannel structures, *Int. J. Heat Mass Transfer*
 601 39 (12) (1996) 2599–2608.
 602 [7] B.X. Wang, X.F. Peng, Experimental investigation on liquid forced
 603 convection heat transfer through microchannels, *Int. J. Heat Mass*
 604 *Transfer* 37 (1994) 73–82.
 605 [8] T.M. Harms, M.J. Kazmierczak, F.M. Gerner, Developing convec-
 606 tive heat transfer in rectangular microchannels, *Int. J. Heat Fluid*
 607 *Flow* 20 (1999) 149–157.
 608 [9] H.J. Park, S.Y. Son, M.C. Choi, G. Lim, I.S. Song, J.J. Pak,
 609 Temperature-dependent property effects on laminar flow character-
 610 istics in a rectangular microchannel, in: *Proceedings of ASME*
 611 *IMECE MEMS-23865*, 2001.
 612 [10] W. Qu, I. Mudawar, Experimental and numerical study of pressure
 613 drop and heat transfer in a single-phase micro-channel heat sink, *Int.*
 614 *J. Heat Mass Transfer* 45 (2002) 2549–2565.
 615 [11] M.N. Sabry, Scale effects on fluid flow and heat transfer in
 616 microchannels, *IEEE Trans. Compon. Packaging Technol.* 23 (3)
 617 (2000) 562–567.
 618 [12] V.K. Samalam, Convective heat transfer in microchannels, *J. Elec-*
 619 *tron. Mater.* 18 (5) (1989) 611–617.
 620 [13] R.W. Knight, J.S. Goodling, D.J. Hall, Optimal thermal design of
 621 forced convection heat sinks—analytical, *J. Electron. Packaging* 113
 622 (1991) 313–321.

[14] R.W. Knight, J.S. Goodling, D.J. Hall, R.C. Jaeger, Heat sink
 623 optimization with application to microchannels, *IEEE Trans. Com-*
 624 *pon. Packaging Technol.* 15 (5) (1992) 832–842.
 625 [15] J.B. Aparecido, R.M. Cotta, Thermally developing laminar flow
 626 inside rectangular ducts, *Int. J. Heat Mass Transfer* 33 (2) (1990) 341–
 627 347.
 628 [16] X. Wei, Y. Joshi, Optimization of stacked micro-channel heat sinks
 629 for micro-electronic cooling, *Int. Soc. Conf. Therm. Phenomena*
 630 (2002) 441–448.
 631 [17] C.P. Tso, S.P. Mahulikar, The use of the Brinkman number for single
 632 phase forced convective heat transfer in microchannels, *Int. J. Heat*
 633 *Mass Transfer* 41 (12) (1998) 1759–1769.
 634 [18] J.M. Li, B.X. Wang, X.F. Peng, ‘Wall-adjacent layer’ analysis for
 635 developed-flow laminar heat transfer of gases in microchannels, *Int. J.*
 636 *Heat Mass Transfer* 43 (2000) 839–847.
 637 [19] G. Tunc, Y. Bayazitoglu, Heat transfer in rectangular microchannels,
 638 *Int. J. Heat Mass Transfer* 45 (2002) 765–773.
 639 [20] S.T. Poh, E.Y.K. Ng, Heat transfer and flow issues in manifold
 640 microchannel heat sinks: a CFD approach, in: *IEEE/CPMT Electron.*
 641 *Packag. Technol. Conf.*, 1998, pp. 246–250.
 642 [21] E.Y.K. Ng, S.T. Poh, CFD Analysis of double-layer microchannel
 643 conjugate parallel liquid flows with electric double-layer effects,
 644 *Numer. Heat Transfer Part A* 40 (2001) 735–749.
 645 [22] A.G. Fedorov, R. Viskanta, Three-dimensional conjugate heat
 646 transfer in the microchannel heat sink for electronic packaging, *Int.*
 647 *J. Heat Mass Transfer* 43 (2000) 399–415.
 648 [23] K.K. Ambatipudi, M.M. Rahman, Analysis of conjugate heat
 649 transfer in microchannel heat sinks, *Numer. Heat Transfer Part A*
 650 37 (2000) 711–731.
 651 [24] H.H. Bau, Optimization of conduits’ shape in microheat exchangers,
 652 *Int. J. Heat Mass Transfer* 41 (1998) 2117–2723.
 653 [25] S.V. Patankar, D.B. Spalding, A calculation procedure for heat, mass
 654 and momentum transfer in three-dimensional parabolic flows, *Int. J.*
 655 *Heat Mass Transfer* 15 (1972) 1787–1806.
 656 [26] J.P. Van Doormaal, G.D. Raithby, Enhancements of the SIMPLE
 657 method for predicting incompressible flows, *Numer. Heat Transfer* 7
 658 (1984) 147–163.
 659 [27] G. Lonsdale, An algebraic multigrid solver for the Navier–Stokes
 660 equations on unstructured meshes, *Int. J. Numer. Methods Heat*
 661 *Fluid Flow* 3 (1993) 3–14.
 662 [28] *CFD-ACE+ Theory Manual*, Version 2002, CFD Research Corpo-
 663 ration, 215 Wynn Drive, Huntsville, AL 35805, 2002.
 664 [29] K. Deb, *Multi-objective Optimization Using Evolutionary Algori-*
 665 *thms*, John Wiley & Sons, 2001.
 666 [30] C.A. Coello Coello, D.A. Van Veldhuizen, G.B. Lamont, *Evolution-*
 667 *ary Algorithms for Solving Multi-objective Problems*, Kluwer Aca-
 668 demic Publishers, 2001.
 669 [31] K. Deb, S. Agrawal, A. Pratap, T. Meyarivan, A fast elitist non-
 670 dominated sorting genetic algorithm for multi-objective optimization:
 671 NSGA-II, in: *Proceedings of the Parallel Problem Solving from*
 672 *Nature PPSN VI*, 2000, pp. 849–858.
 673 [32] K. Deb, A. Pratap, S. Agarwal, T. Meyarivan, A fast and elitist
 674 multiobjective genetic algorithm: NSGA-II, *IEEE Trans. Evol.*
 675 *Comput.* 6 (2) (2002) 182–197.
 676 [33] T. Okabe, Y. Jin, B. Sendhoff, Evolutionary multi-objective optimi-
 677 sation with a hybrid representation, in: *Proceedings of the IEEE*
 678 *Congress on Evolutionary Computation CEC*, 2003, pp. 2262–2269.
 679 [34] L. Piegler, W. Tiller, *The NURBS Book*, second ed., Springer, 1997.
 680 [35] T. Okabe, K. Foli, M. Olhofer, Y. Jin, B. Sendhoff, Comparative
 681 studies on microheat exchanger optimisation, in: *Proceedings of the*
 682 *IEEE Congress on Evolutionary Computation CEC*, 2003, pp. 647–
 683 654.
 684 [36] T. Okabe, *Evolutionary Multi-objective Optimization—On the Dis-*
 685 *tribution of Offspring in Parameter and Fitness Space*, Shaker Verlag,
 686 2004, ISBN 3-8322-2904-3.
 687
 688